Applied Acoustics 205 (2023) 109277

Contents lists available at ScienceDirect

Applied Acoustics

journal homepage: www.elsevier.com/locate/apacoust

Calculating the equivalent elastic moduli and their influence on modelling the sound insulation of softwood cross laminated timber (CLT)

Claire Churchill [a,1,*], Bernd Nusser [b], Christian Lux [b]

[a] Institute of Material Technology, Building Physics, and Building Ecology, TU Wien, Karlsplatz 13, 1040 Wien, Austria
[b] Holzforschung Austria, Franz Grill-Strasse 7, 1030 Wien, Austria

ARTICLE INFO

Article history:
Received 1 April 2022
Received in revised form 20 January 2023
Accepted 10 February 2023
Available online 24 February 2023

Keywords:
Cross-laminated Timber (CLT)
Layered structures
Orthotropy
Sound insulation
Thick plate
Wood

ABSTRACT

There are characteristics unique to natural materials such as timber that must be dealt with carefully to develop successful sound insulation prediction models. Timber has low internal losses typical of low-density building materials but with material properties that vary according to growth conditions. To study these factors in cross laminated timber (CLT) products, orthotropic thin plate and isotropic thick plate models are investigated. Equivalent elastic moduli are obtained using two methods from values and limits provided in the timber standards and literature, or by the manufacturer. The equivalent moduli are used to calculate the sound insulation of three- and five-layer CLT plates. Appropriate upper and lower limits are calculated from the combined material parameters and compared with sound insulation results measured in accredited laboratories for the first time. EN ISO 10140 test standards require that surface density of the sample be documented in the laboratory; additional precision information such as the fifth percentile of the material density is not required. However, considering the limits on the internal loss factors and elastic moduli only in the thin plate sound insulation model, gives a poor overall prediction performance (23.6% within the upper and lower limits). In this paper we combine the limits on elastic moduli, internal loss factors, and density. With these combined parameters the prediction is improved; less than half of the measured sound insulation values fall within the upper and lower limits of a typical thin plate model (44.0%). The single figure sound reduction index values are underestimated in seven out of nine cases. The prediction is further improved when a thick plate model is considered. There are several layers of complexity in the measurement and modelling conditions that must be carefully considered. The contributions from these compounding factors are discussed, and additional moduli and density parameters are proposed for inclusion in the literature and standards.

1. Introduction

The debate about whether we should grow building materials, because of carbon sequestering potential, or modify building manufacturing processes to lower environmental impact is ongoing [1–3]. A pluralistic approach to solve environmental issues, with sustainable wood products securing a share of the market is the likely outcome. Timber is a low-density product when compared with brick or concrete. This affords some advantages in construction where cross-laminated timber (CLT)[2] or other solid timber products are used, such as, enhanced prefabrication possibilities [4–6]. Key building physics aspects to the adoption of sustainable timber as a principle building material are fire safety, moisture transfer, and vibration and sound insulation performance. The aim of this work is to assess the efficacy of infinite plate theory to predict the airborne sound insulation (50–5000 Hz) of CLT panels using equivalent elastic moduli. CLT is a common name "for sheets, panels, posts and beams made of glued boards or planks layered alternately at right-angles" [7]. Such products are usually symmetrical through the cross-section and consist of an odd number of layers. There are four main problems unique to solid timber panels, such as CLT, that must be resolved to develop successful sound insulation prediction models.

(1) The internal loss factors of wood products are low: in some frequency bands, the radiation coupling losses may exceed the internal loss factor. This is characteristic of many lightweight

* Corresponding author.
E-mail addresses: claire.churchill@tuwien.ac.at, c.e.churchill@salford.ac.uk (C. Churchill).
[1] Present address: Acoustics Research Centre, Newton Building, University of Salford, Salford, Greater Manchester, M5 4WT.
[2] *Abbreviations*: CLT, cross-laminated timber.

https://doi.org/10.1016/j.apacoust.2023.109277
0003-682X/

materials and, consequently, the internal loss factor of these materials is difficult to measure.

(2) Solid wood construction is a low-density building material, particularly where softwood is the principal raw material. The material is organic, and the density varies according to growth conditions. The fifth percentile of the material density may provide a measure of this variability [7], however this metric is not commonly expressed in the literature [8–10]. Density metrics to determine the mass loading are provided for structural safety. However, the problem of defining the most appropriate density metrics for application to acoustic modelling problems should be studied further. The low density of timber also means that the critical frequencies of radiating CLT panels fall within the building acoustic range (50–5000 Hz). The critical frequency (f_c) is the lowest frequency for which there is phase matching of the bending wave on the plate and the longitudinal wave in the air, resulting in high radiation power losses to the air; this occurs at grazing incidence (i.e., when the incoming or outgoing longitudinal wave is parallel to the plate). As described in bullet point (1) the radiation coupling losses may in fact exceed the internal loss factor and make the internal loss factor difficult to measure. When the critical frequency falls within the building acoustic range, the diffuse sound insulation properties must be described by a combination of energy transfer processes categorised as both lightweight (governed by the mass) and heavyweight (governed by the loss factor). Thus, increasing the complexity of the modelling problem to be considered. These categories are used to distinguish between partition material types in the building acoustics standards [11–13].

(3) Timber is an orthotropic material; a natural material, the elastic modulus varies according to growth conditions. The fifth percentile of the elastic modulus in the direction parallel to the grain is the parameter used to express this variation [9]. The way in which the material is assembled in the panel has the side effect of reducing orthotropy. Where some orthotropy remains, the characteristic plot of diffuse sound insulation against the frequency has two dips that can be attributed to the corresponding critical frequencies (f_{c1} and f_{c2}) in the orthogonal material directions (see Fig. 1). If a panel has particularly different bending stiffnesses in the orthogonal directions, such as the case with the material depicted in Fig. 1, this also results in an extended region of poor sound insulation between the two critical frequencies.

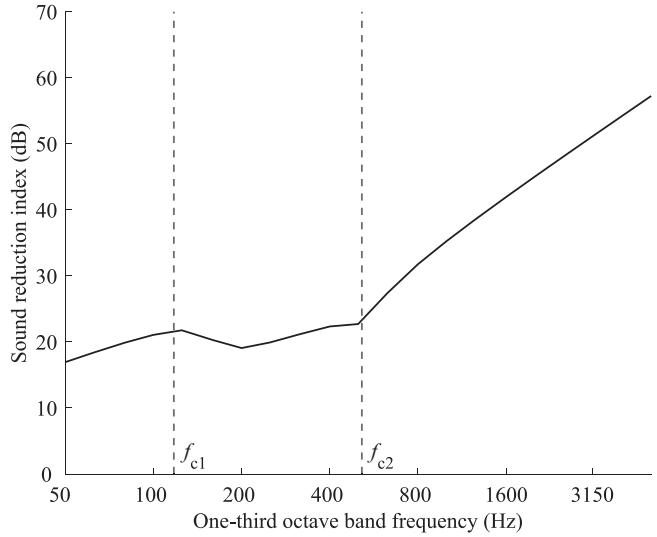

Fig. 1. Calculated diffuse sound reduction index for an orthotropic material. (CLT with elastic moduli $E_{eq,x}$ = 7.4x10^8 Nm^{-2} and $E_{eq,y}$ = 1.4x10^{10} Nm^{-2}.) The calculated critical frequencies are marked f_{c1} and f_{c2}.

(4) The orthotropic behaviour of timber also includes low shear moduli; this may mean a transition to thick plate behaviour within the building acoustics range. The principal energy transfer processes discussed thus far assume thin plate models; a transition to a thick plate model introduces additional energy transfer mechanisms.

Sound insulation calculations [14] are not as sensitive to changes in the dynamic elastic modulus as static and dynamic failure applications [15,16]. Reducing the elastic moduli E_x and E_y by 50 % results in deviations in the single figure sound reduction index (R_W) of 0.0 dB to 2.0 dB. Deviations in third octave band insulation of up to 4.3 dB (where $f > f_{c2}$) are also observed and the first modal frequency of the simply supported plates is shifted by one to two third octave bands. Transition to a thick plate model within the frequency range of interest (50–5000 Hz) is evidenced by a plateau in sound insulation corresponding to the dispersion relation of the bending wave; the dispersion relation relates the phase velocity to frequency. The plateau observed in sound insulation of thick concrete or masonry plates may be modelled with a frequency-dependent modulus based on the dispersion relation of the bending wave [17,18]. However, the frequency-dependent modulus of these materials is calculated using the assumption of an isotropic plate material; in an orthotropic material such as CLT, the dispersion curves may plateau at different frequencies in different material directions [19]. To model the effect in the orthotropic case, the dynamic material properties can be adjusted in the calculation to obtain a best fit with measured sound insulation data, thus obtaining a frequency-dependent modulus. However, adopting a pragmatic approach to adjust the material parameters can lead to difficulties, particularly if the selected parameters do not fall within a reasonable allowable range. Following this approach may lead to incorrect assumptions about the validity of models or limited success in the prediction of more complicated panel designs, which include CLT layers.

This study investigates the feasibility of using measured material parameters taken from the literature or, where possible, measured directly in the laboratory to predict the sound insulation of nine different CLT plates. Infinite plate theory for orthotropic thin and isotropic thick plates taken from the literature are used. The plates are from five different manufacturers, consisting of either three or five material layers. Section 2 gives a brief overview of methods to determine the elastic moduli. Section 3 describes in detail the methodologies implemented to calculate the elastic moduli, the sound insulation, and the radiation coupling. Two methods for calculating the equivalent modulus of elasticity are evaluated. One method is selected as the most appropriate for the in-depth study. The radiation coupling of the plate is required to validate the loss factor measurements and is discussed further below. The properties of the plate samples are described in detail in section 4. This includes calculated equivalent plate moduli, shear moduli, and typical densities of softwoods. The percentage difference in equivalent modulus of elasticity calculated incorporating the fifth percentile of the elastic modulus in the direction parallel to the grain is compared with the percentage difference in equivalent modulus calculated using the gamma theory. The first method is further explored for all plates also including the maximum possible range of plate densities taken from the literature. The limitations of using the mass per unit area measured/recorded in the lab to calculate the sound insulation are discussed (specifically for plates 1, 3 and 6–9). Section 4 describes the measurement procedures to determine the loss factor and the sound insulation. The loss factor of plate 1 was measured while hanging freely in the laboratory. The sound insulation of plate 1 is predicted using this measured loss factor. The limits on this measurement method are discussed and the sound insulation prediction based on a literature value is provided for comparison. The internal loss

factor is a key input parameter for the sound insulation models and is also used to determine the modal overlap factor. The expected standard deviation of velocity levels or coupling loss factors in structure-borne applications can also be calculated from the modal overlap factor. This provides an additional measure of the applicability and appropriateness of different sound insulation calculation models. The measured loss factor results of plate 1 were used to determine modal overlap factors of all the plates [20]; low modal densities can lead to prominent modes which dominate the sound insulation. The sound insulation measurements of the nine plates were measured in the various transmission suites of two different acoustic laboratories. The results and conclusions are presented and discussed in sections 5 and 6.

2. Brief overview of methods to determine the elastic moduli

Methods to obtain the elastic moduli of a panel include measurements of static deflections, a variety of non-destructive test methods, and material property calculations. Test methods can vary in size and scope, ranging from small-sample testing of the raw wood materials (e.g., Young's moduli in tension, or compression, shear moduli, and Poisson's ratio [10,21–24]) to large scale beam or panel testing (e.g., ultrasonic testing [25] and modal testing [26–28]). Measurements can take place under different environmental conditions to quantify the effect of factors such as moisture content, wood seasoning, shrinkage, or time dependency (e.g., creep) [10,22,29]. These methods are useful not only to provide insights into material grading for strength, failure, and additional non-linear applications but also to assess the properties of wood in applications where small linear deflections are relevant. This includes subjective perception and human response to building vibration (e.g., whole-body vibration, periodicity of footfalls, vibration induced rattle, annoyance, sleep disturbance etc. [30–32]) or sound insulation [33]. Concurrent acoustic and vibroacoustic design of layered materials requires that the underlying relationship between low frequency vibroacoustic (f < 40 Hz) material properties [31] and the high frequency acoustic (f > 50 Hz) material properties [18] is defined. Rather than fitting dynamic elastic moduli to align tentative models to measured data, such as sound insulation performance, developing optimised direct and flanking transmission models that incorporate calculated and measured material properties are a preferred solution [33,34].

There are a variety of calculation methods to determine the elastic moduli based on beam theories applied to the plate. Zhou et al. [26] identify these primary techniques:

- The k-method makes use of a transformed cross section to determine an equivalent elastic modulus [10].
- The shear analogy method is based on a moment of area calculation to determine the equivalent elastic and shear constants [10]. This is like the gamma method but with the correction factor set to one, γ = 1.0. From these constants a frequency-dependent apparent modulus of elasticity can be determined [26]. The frequency-dependent modulus depends on loading conditions.
- The gamma method applies correction factors (γ) to the moment of area calculation to account for shear deformation of the layers [8].

These methods are all based on determining equivalent moduli, which may involve the introduction of correction terms. The approaches described have already proven successful in structural applications involving CLT panels [15]. In previous studies, the calculated values of the equivalent static elastic moduli would be expected to deviate from the measured dynamic elastic modulus by no more than E_x(+11 %, −13 %), E_y(+49 %, −33 %) (or up to E_y(+60 %) [35], the large difference being attributed to defects such as knots, "pitch pockets," and irregular grain patterns) [26,27,35,36]. Pitch pockets are cavities in the wood grain caused by insects or an impact, which subsequently fill with resin.

There are several methods to manufacture solid wood panels such as CLT. The type of wood used in the panel, moisture content, workmanship, and assembly procedures such as edge bonding, gaps (e.g. intentional due to lack of edge bonding [26] and unintentional due to shrinkage [29] or delamination [27]), stress relief cuts in the core layer, and the use of solid wood panels rather than lamellas [26,27,35] can lead to different mechanical properties. The moisture content of these finished wood products can also vary, with 10–18 % a typical range for which the elastic moduli are adjusted [29].

3. Methodology

The equivalent modulus of elasticity was determined for the nine plates using two methods. The first method does not account for the shear deformation of the core layer, and the second method applies a simple correction to account for this effect. The data for panels 2 to 9 was anonymised, and therefore panel wood types, wood moisture content, workmanship, and assembly procedures were not considered. Whether these additional factors, which cannot be fully accounted in the methods described, could lead to differences in the dynamic modulus of elasticity large enough to significantly influence sound insulation is, in the light of previous studies, unlikely [35,37,38]. The equivalent elastic moduli were then used to calculate the sound insulation of the plate using two models: an orthotropic thin plate model (see section 2.2) and an isotropic thick plate model (see section 2.3). The study on the input data was confined to simple infinite plate models so that the effects of the input data could be clearly compared. In both models and all plate cases, it was assumed that an infinite plate would be sufficient to model the sound insulation. Maximum and minimum limits of the models were calculated using the fifth percentile of the elastic modulus (in the direction parallel to the grain), the range of values of wood density, and the internal loss factor provided by literature [39]. The models were compared with sound insulation results measured in accredited laboratories. The equivalent modulus of elasticity was also used to determine the bending modes of the plates with the assumptions of free and simply supported boundary conditions in all third octave frequency bands. Thus, the modal densities in each third octave band can be computed and, together with the loss factor of the plate, can be used to determine the modal overlap factors within each third octave band. The number of modes and the modal overlap factors can also be used to determine the expected standard deviation in structure-borne applications within each third octave band. These calculations are described further in section 4.1.3.

To correctly determine the sound insulation, the internal loss factor of the plate is required in addition to the modulus of elasticity. Therefore, the structural reverberation times of plate 1 were measured and the internal loss factor of this plate was obtained. These measured loss factors are compared with values provided in the literature [39]. The internal loss factors of lightweight materials are high ($\eta_{\text{internal}} \geq 0.01$), and therefore the structural reverberation times are short and difficult to measure. The bending wave on the plate is dispersive and thus radiates efficiently in the region of the critical frequency. The internal loss factor may therefore be obscured by radiation losses from the plate in the region of the critical frequency [40]. The result is compared with the calculated radiation loss factors (section 2.4 and appendices

D, E, F and G for details) to examine the validity of the measurement.

3.1. Equivalent modulus of elasticity

The methods to calculate the total bending stiffness of layered panels, such as those presented in the introduction, make use of an equivalent bending strain energy component [10] to determine an equivalent homogenous material throughout the cross section. While these calculations are commonly applied to beams, they are also relevant for layered plates and can be divided into two main approaches. The first approach is to transform the cross-sectional area of the layers by increasing or decreasing the layer width to an equivalent value. The k-method described in the introduction is an example of such an approach. There are several reasons why the k-method is difficult to apply to layered CLT plates: not only is the layer width large in the case of a plate when compared to a beam, but the method also requires the calculation of equivalent shear moduli. Detailed in-plane and out-of-plane shear moduli are not commonly provided for CLT plates, and therefore this approach was not considered further. The second approach is to sum the bending stiffnesses ($B = E_{eq}I$) of the layers to reach an equivalent modulus for the whole cross section. If the layers of the CLT plates are assumed to be perfectly bonded with no shearing between the layers or of the core material, the equivalent modulus of elasticity of a layered plate is then given by [10]:

$$E_{\mathrm{eq}} = \frac{2}{I}\sum_{i=1}^{n} E_{Li} I_i \tag{1}$$

where I is the total second moment of area of the beam or plate, E_{Li} is the elastic modulus of layer i, and I_i is the moment of inertia of each lamina given by parallel axis theorem. The layers, i, are numbered from the middle surface, and therefore n is half the number of layers and the thickness of the first layer h_1 is one half the thickness of the middle layer.

$$I_i = I_{0i} + h_i d_i^2 \tag{2}$$

where I_{0i} is the moment of inertia of layer i and d_i is the distance to the neutral plane. The sound insulation is determined by substituting the equivalent moduli directly into the sound insulation models as described in sections 2.2 to 2.4.

The equivalent modulus of elasticity would be expected to decrease in the direction of the highest bending stiffness as the corresponding aspect ratio, L_y/h or L_x/h, decreases [27]. Using a similar approach but accounting, in this instance, for shear deformation of the core layers, gamma theory is applied to panels with three and five layers. In a similar way to mechanically jointed beams that are symmetrical about the neutral plane, the equivalent modulus is given by [8,15,16]:

$$E_{eq,\gamma} = E_{eq} + \frac{\Delta E_{eq,\gamma}}{100} E_{eq} = \frac{2}{I}\sum_{i=1}^{n} E_{Li}(I_{0i} + \gamma_i h_i d_i^2) \tag{3}$$

The factor, γ_i, must be modified to account for shear deflection of bonded core layers rather than mechanical slippage. The modifying factor described in appendix A has been applied in situations with concentrated loadings where CLT panels are tested to failure (for example [15]), and could be expected to present a worst case scenario in acoustic problems. In the case of airborne sound insulation measurements small deflections and linear elasticity are assumed which are well within the extremes of panel failure [41,42]. Additional factors such as panel assembly procedures and connection methodologies could be included in the gamma correction, however, the assembly methods must be clearly delineated with the agreement of the manufacturers, therefore these factors were not examined on a case-by-case basis for individual panels at this time.

3.2. Orthotropic thin plate model of sound insulation

The orthotropic model is an infinite thin plate model integrated over all angles of incidence (ϕ, θ) [41,42]:

$$\tau_{\infty,d} = \frac{2}{\pi}\int_0^{\pi/2}\int_0^{1} \frac{\mathrm{d}\left(\sin^2\theta\right)\mathrm{d}\phi}{\left|1+\frac{Z\cos\theta}{2\rho_0 c_0}\right|^2} \tag{4}$$

where $\tau_{\infty,\mathrm{d}}$ is the diffuse incidence transmission coefficient, Z is the surface impedance, ρ_0 is the density of the gas (air), and c_0 is the speed of sound in the gas (air). The surface impedance of a thin plate is provided in appendix B. The integral in Eq. (4) was calculated numerically using the iterated method of the MATLAB double integral function and the sound insulation was calculated according to:

$$R_{\mathrm{orth}} = -10log\frac{1}{\tau_{\infty,d}} \tag{5}$$

3.3. Isotropic thick plate model of sound insulation

The isotropic thick plate model is implemented similarly to the orthotropic thin plate model but with an isotropic bending stiffness (see appendix B) and a correction to account for the thick plate. The thick plate correction based on Ljunggren is given by [43].

$$R_{\mathrm{thick}} = R_{\mathrm{iso}} - \Delta R_{\mathrm{c}} \tag{6}$$

where R_{iso} is the calculated isotropic thin plate sound insulation and the correction term (ΔR_{c}) is dependent on E_{iso}, h, ρ and ν, the calculation is provided in appendix C. The estimate for the isotropic shear constant was given by

$$G_{\mathrm{iso}} \approx \frac{E_{\mathrm{iso}}}{(1+\nu)} \tag{7}$$

where $E_{\mathrm{iso}} = 12(1\text{-}\nu^2)B_{\mathrm{iso}}/h^3$ (see appendix B for a definition of B_{iso}) and Poisson's ratio, ν, is estimated to be 0.12. When compared with the shear constants of raw material timber the isotropic shear constant is overestimated ($G_{\mathrm{iso}} > G_{\mathrm{TR}}|\, G_{\mathrm{LR}}|\, G_{\mathrm{LT}}$ [10]). The thin plate limit can be calculated by [39]:

$$f_{\mathrm{B(thin)}} = \frac{0.05 c_{L,p}}{h} \tag{8}$$

where $c_{\mathrm{L,p}}$ is the longitudinal phase velocity of the panel material and h is the thickness of the panel. The isotropic longitudinal phase velocity of the panel is estimated by

$$c_{L,p} = \left(\frac{E_{\mathrm{iso}}}{\rho(1-\nu^2)}\right)^{(1/2)} \tag{9}$$

where ρ is the density of the panel.

3.4. Estimating the radiation coupling

The radiation coupling of the plate can be estimated by the following equation [39]:

$$\eta_{\mathrm{ij}} = \frac{\rho_0 c_0 \sigma_i}{\omega \rho_{s,\mathrm{i}}} \tag{10}$$

where ω is the angular frequency, $\rho_{\mathrm{s,i}}$ is the surface density of the plate, and the radiation efficiency (σ_{i}) of an isotropic plate (i) with various boundary conditions can be estimated for infinite,

baffled finite, and unbaffled finite thin plates. A loss factor ($\eta = \eta_{rad} + \eta_{int}$) measured as described in section 4.1 will always consist of the internal loss factor, η_{int}, plus the radiation coupling, η_{rad}. If radiation losses are comparable to the internal loss factor ($\eta_{rad} \geq \eta_{int}$) they will influence the measured result. For this reason, the radiation losses for different plate boundary conditions are estimated.

3.4.1. Finite baffled thin plate radiation

The radiation efficiency of a baffled plate with simply supported and clamped edge conditions is given in appendix D. The radiation efficiency is found to increase as the boundary conditions become more constrained. The maximum value of this expression is given by [44]:

$$\sigma_{max} = \begin{cases} \frac{U}{2\pi\mu k S\sqrt{\mu^2-1}}\left[\ln\left(\frac{\mu+1}{\mu-1}\right)+\frac{2\mu}{\mu^2-1}\right]\left[4-3\mu^{-8}\right] & (f < f_c) \\ \left(0.5-\frac{0.15L_1}{L_2}\right)\sqrt{k}\sqrt{L_1} & (f = f_c) \\ \frac{1}{\sqrt{1-\mu^2}} & (f > f_c) \end{cases} \quad (11)$$

where the plate has clamped edges and perpendicular baffle conditions. L_1 is the smaller and L_2 is the larger of the rectangular plate dimensions, L_x and L_y, $= \sqrt{f_c/f}$, U is the plate perimeter, and S is the plate area. The radiation efficiency for the frequency band that contains the critical frequency in Eq. (11) can be calculated using $k = 2\pi f_c/c_0$, where f_c is the critical frequency of the plate (see appendix G) and c_0 is the speed of sound in air. The lowest radiation efficiency is given by free boundary conditions. However, free boundary conditions also imply a baffle-free plate and the radiation efficiency of such plates is discussed further in section 2.4.2 below. When substituted into Eq. (10) the radiation coupling loss factor η_{ij} describes the radiation from one side of the plate only. In this case, the loss factor must be multiplied by two to describe the total radiation losses.

3.4.2. Finite unbaffled thin plate radiation (free boundary conditions)

Radiation from a plate with free boundary conditions is determined from the radiation interaction between line and point sources at the edges of the plate. The radiation efficiency is therefore given by the following equation [45]:

$$\sigma_{min} = F_{plate}\left(F_{corner}\sigma_{corner} + F_{edge}\sigma_{edge}\right) \quad (f < f_c) \quad (12)$$

where σ_{corner} is the radiation efficiency of the plate corners (see appendix E), σ_{edge}, is the radiation efficiency of the plate edges (see appendix E), F_{plate}, F_{corner} and F_{edge} are correction factors due to the interaction between the power flows on each side and around the perimeter of the plate (see appendix F). This describes the radiation from both sides of the plate and can be substituted directly into Eq. (10) to give the total radiation coupling losses.

3.4.3. Infinite thin plate between the critical frequencies

An estimate for the frequency-average radiation efficiency for one-third octave bands between the two critical frequencies of the orthotropic plate is given by [42]:

$$\sigma_{ortho} = \frac{1}{\pi^2}\sqrt{\frac{f_{c1}}{f_{c2}}}\left(\ln\frac{4f}{f_{c1}}\right)^2 \quad (13)$$

where f_{c1} and f_{c2} are the critical frequencies in the orthogonal directions (see appendix G). When substituted into Eq. (10), the radiation coupling loss factor η_{ij} describes the radiation from one side of the plate only. Therefore, the loss factor must be multiplied by two to describe the total radiation losses. This result is the lowest radiation coupling of the three radiation efficiencies described ($\sigma_{ortho} < \sigma_{min} < \sigma_{max}$).

4. Sample descriptions

All panels were made from softwood and it is assumed that all panel materials met strength class C24 requirements [9]. The material of panel 1 had elastic stiffnesses surpassing the minimum requirement, with elastic moduli in the parallel and perpendicular directions to the grain of E_{ll} = 12.0x10^9 Nm^{-2}, and $E_{\perp}$=4.0x10^8 Nm^{-2} respectively; these stiffnesses were provided by the manufacturer. The variability of the modulus was considered using the fifth percentile of the elastic modulus in the direction parallel to the grain for strength class C24. Panels 2 to 9 were assumed to have elastic moduli equal to Douglas fir (12 % moisture content, taken from the literature [10]), and therefore $E_{ll} = E_L$ = 14.5x10^9 Nm^{-2}, and $E_{\perp}=(E_R + E_T)/2=(0.96 + 0.09)/2$ x10^9 Nm^{-2} = 5.25x10^8 Nm^{-2}, where E_L, E_R, and E_T are the stiffnesses of the timber in the radial and tangential material directions of the log respectively. Note that in Eurocode 5 [8], the elastic directions parallel (E_{ll}) and perpendicular ($E_{\perp}$) to the grain are only considered, and therefore $E_{\perp}$ is assumed to be the mean of the tangential and radial material directions. The calculated equivalent plate data, assumed values for G_{xy}, plate thicknesses, aspect ratios, and densities recorded in the laboratory are listed in Table 1. Sound insulation data for plate 9 were measured using two aspect ratios and both are also listed in Table 1. The density and the shear modulus, G_{xy} of plate 1 were measured in the laboratory. The quoted density of plate 6 is the mean of four nominally identical plates and includes the fifth percentile of whole panel measurements. (Note that the fifth percentile of the material density, like the fifth percentile of the elastic modulus in the direction parallel to the grain

Table 1
Calculated equivalent plate data.

Plate	Manufacturer	$E_{eq,x}$ (Nm^{-2}) Eq. (1)	$E_{eq,y}$ (Nm^{-2}) Eq. (1)	G_{xy} (Nm^{-2})	Thickness (m)	Aspect ratios (-) L_x/h	L_y/h	Density (kgm^{-3})
1	A	3.232 × 10^9	9.168 × 10^9	[2]6.2 × 10^8	0.080	52.3	36.1	438
2	B	1.997 × 10^9	1.303 × 10^{10}	–	0.072	50.4	41.0	–
3	B	1.186 × 10^9	1.384 × 10^{10}	–	0.094	38.6	31.4	479
4	B	2.440 × 10^9	1.259 × 10^{10}	–	0.128	28.4	23.0	–
5	B	3.764 × 10^9	1.126 × 10^{10}	–	0.158	23.0	18.7	–
6	C	1.043 × 10^9	1.398 × 10^{10}	[3]6.9 × 10^8	0.090	29.7	44.1	[5]472 ± 8.6
7	D	1.584 × 10^9	1.344 × 10^{10}	–	0.140	30.2	37.4	464
8	D	4.601 × 10^9	1.042 × 10^{10}	–	0.120	43.7	35.3	470
9	E	1.419 × 10^9	1.361 × 10^{10}	–	0.100	[4]36.3/52.4	[4]29.5/42.3	480

[2] Measured.
[3] Provided by the manufacturer.
[4] Two aspect ratios were used.
[5] Mean and fifth percentile determined from four nominally identical plates.

[9] can be much larger.) The shear modulus was measured from an assessment of measured and calculated modes. The G_{xy} for plate 6 was provided by the manufacturer and was assumed, in the absence of this data for the other plates (2 to 9), to be the same for all other plates when calculating the principal modes and modal densities. The shear modulus, G_{xy}, was not required to predict the sound reduction index.

The out-of-plane shear moduli for calculating the modified elastic constants due to modified gamma theory were also taken from the literature (Douglas fir, 12 % moisture content [10]). The simplified geometry assumptions for these moduli are summarised pictorially in Fig. 2, and therefore $G_{\perp}$=G_{RT} = 8.0x10^7 Nm^{-2} and G_{ll}=(G_{LT} + G_{LR})/2=(8.3 + 7.6)/2 x10^8 Nm^{-2} = 7.95x10^8 Nm^{-2}. Simplifying assumptions have been made to describe the constants in terms of the elastic directions parallel (E_{ll}) and perpendicular ($E_{\perp}$) to the grain. These assumptions were necessary, to enable values from the literature to be used. Precision shear moduli are not commonly supplied for CLT panels and would not be expected to significantly alter the calculated equivalent elastic moduli. Using the calculation methods and panel sizes described here a ± 50 % change in $G_{\perp}$ would be expected to affect the calculated equivalent elastic modulus, E_x, by ~ 0.04 %. and a ± 50 % change in G_{ll} would be expected to affect the calculated equivalent elastic modulus, E_y, by ~ 12 %. The percentage differences in E_x and E_y when using modified gamma theory and the fifth percentile of the elastic modulus in the direction parallel to the grain are listed in Table 2. In this latter case substituting E_{Li} for E_{Li} ± $\Delta E_{Li,0.05}$, in appropriate layers where $\Delta E_{Li,0.05}$ is the fifth percentile of the elastic modulus in the direction parallel to the grain to obtain $E_{eq,0.05}$ in Eq. (1) which can also be expressed by:

$$E_{eq,0.05} = E_{eq} \pm \frac{\Delta E_{eq,0.05}}{100} E_{eq} \tag{14}$$

Two values are listed for plate nine, corresponding to the two different plate sizes measured. The equivalent elastic moduli for the five-layer plates are not significantly more reduced than the three-layer plates. This may be because the modified gamma method only considers the outer layers of the five-layer plates. The minimum, maximum and assumed values of the density of softwoods are taken from the literature [10]. The minimum is the value for US northern white cedar, the assumed is the value for Sitka spruce (commonly grown in Europe for the construction industry) and the maximum is the value for Canadian western larch. The densities of these softwoods are listed in Table 3.

Note that the areas of the plates all conform to allowable plate sizes according to the test standard EN ISO 10140 [11]. The standard specifies a surface area >10 m^2 and a minimum dimension L_x | L_y>2.3 m. This aims to provide partition sizes typical of that in a real building with an aspect ratio (L_x/L_y) that avoids degenerate modes if the materials are isotropic. Whether or not all orthotropic building materials, such as CLT, will always fulfil the criteria of avoiding degenerate modes with these specifications is uncertain. In this work, none of the plates selected for testing were anticipated to exhibit degenerate mode behaviour. Finally, the calculated thin plate limits for each of the plates and the data used to perform these calculations including the assumed densities for each of the

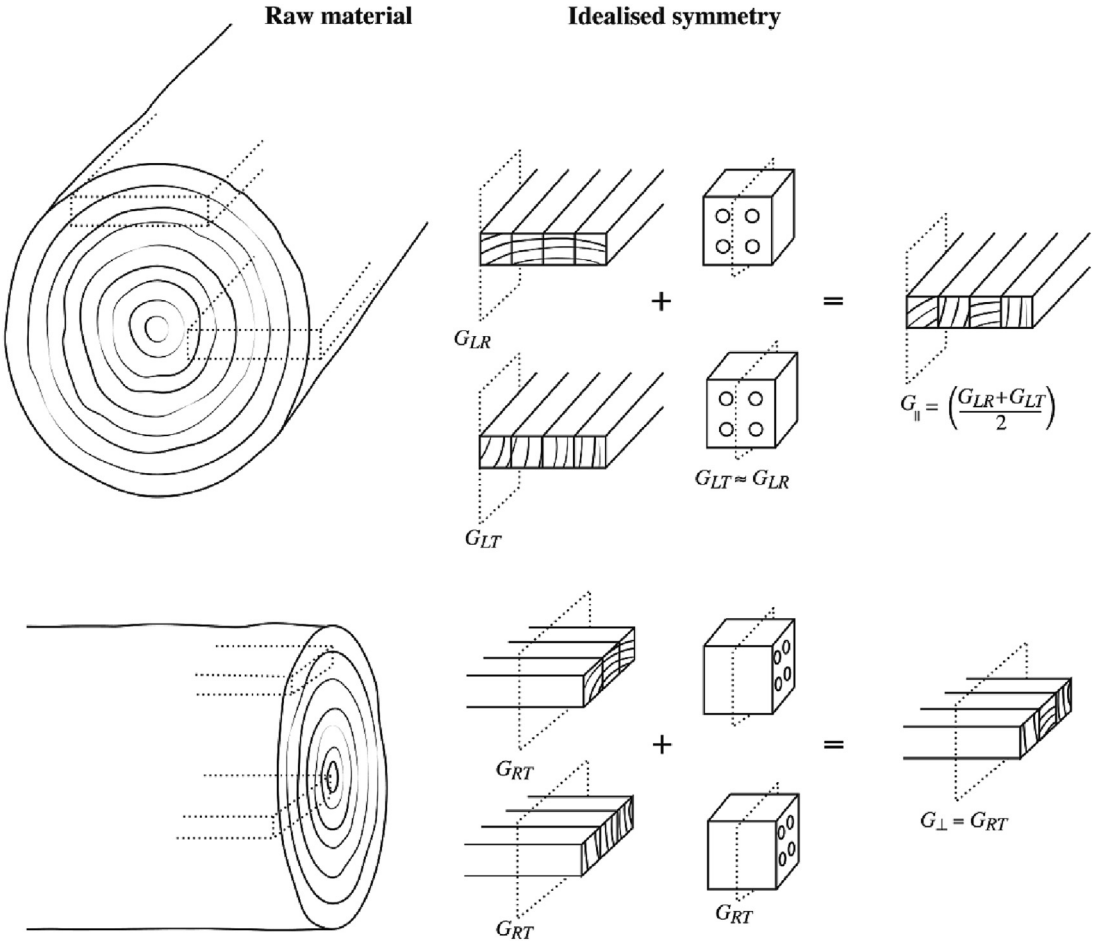

Fig. 2. Geometry assumptions for the out-of-plane shear moduli.

Table 2
Percentage differences in the equivalent elastic modulus when using modified gamma theory and the fifth percentile of the elastic modulus in the direction parallel to the grain.

Plate	Manufacturer	$\Delta E_{eq,x,\gamma}$ (%)	$\Delta E_{eq,y,\gamma}$ (%)	$\Delta E_{eq,x,0.05}$ (%)	$\Delta E_{eq,y,0.05}$ (%)	No. of layers
1	A	−0.002	−11.41	±16.3	±17.8	3-layer
2	B	−0.007	−11.19	±39.0	±50.8	3-layer
3	B	−0.020	−16.12	±29.5	±50.9	3-layer
4	B	−0.005	−9.961	±41.6	±50.7	5-layer
5	B	−0.005	−16.69	±45.6	±50.5	5-layer
6	C	−0.037	−8.543	±26.3	±51.0	3-layer
7	D	−0.008	−4.674	±35.4	±50.9	5-layer
8	D	−0.001	−5.467	±46.9	±50.3	5-layer
9	E	[2]-0.019/ −0.009	[2]-18.60/ −10.07	±33.3	±50.9	3-layer

[2] Two aspect ratios were used.

Table 3
The density of softwood [10].

	Species	Growing territory	Density (kg/m^3)
Min	Northern white cedar	US	290
Assumed	Sitka spruce	US	380
Max	Western Larch	Canada	550

plates is listed in Table 4. The assumed shear constant, G_{iso}, calculated according to Eq. (7) required for the isotropic thick plate model are also included for comparison.

5. Measurement methods

5.1. Loss factor

The internal loss factor of the CLT plate is required to calculate the airborne transmission at frequencies greater than the critical frequency. An estimate of internal loss factor was made from the measured structural reverberation times of plate 1 while the plate was freely hanging in the laboratory. The plate was suspended in the laboratory space from a single point using a hole drilled 20 cm from the upper edge at the top of the plate. This was attached to the laboratory crane to minimise coupling losses, although plate-to-room coupling losses are unavoidable in this situation. Acceleration decays from an impulse measurement were recorded with a two-channel digital recorder (Sound Devices 702 T). Two accelerometers (B&K Type 4513-B) were used to record the decay signal and a large hammer (4.8 kg) was used to excite the wall. The signal was processed to obtain the structural reverberation time from a T_5 measurement [40] and determine the loss factors. To validate the loss factor measurement, the results are compared with the calculated plate-to-room losses. The plate-to-room losses are calculated using the minimum, maximum and orthotropic calculated radiation efficiencies as described in section 2.4.

Table 4
Calculated thin plate limits and the assumed shear constants, thickness, and densities used to estimate the limits.

	G_{iso} (Nm^{-2}) Eq. (7)	Thickness (m)	Density (kgm^{-3})	Thin plate limit (Hz) Eq. (8)
Plate 1	2.1×10^9	0.080	[2]438	2205.8
Plate 2	2.0×10^9	0.072	[3]380	2547.0
Plate 3	1.6×10^9	0.094	[3]380	1738.8
Plate 4	2.1×10^9	0.128	[3]380	1493.4
Plate 5	2.5×10^9	0.158	[3]380	1311.3
Plate 6	1.5×10^9	0.090	[3]380	1763.0
Plate 7	1.8×10^9	0.140	[3]380	1245.9
Plate 8	2.7×10^9	0.120	[3]380	1780.7
Plate 9	1.7×10^9	0.100	[3]380	1702.2

[2] Recorded in the lab (see Table 1).
[3] Assumed (Sitka spruce, see Table 3).

To determine the applicability and appropriateness of different sound insulation calculation models, the first few modal frequencies of the plates with free edges and simply supported conditions were calculated. The modal overlap factor was calculated according to [20,39]:

$$M = f\frac{N\eta}{\Delta f} \tag{15}$$

where N is the number of modes (determined analytically) in the third octave band, Δf is the width of the band, and η is the measured total loss factor. To determine the sound insulation in a building, the direct sound insulation discussed thus far is not always the principal energy transfer path. Flanking paths due to structural coupling provide additional energy transfer between rooms. Therefore, the expected standard deviation of velocity levels or coupling loss factors in structure-borne applications, σ_{dB}, is also quantified [20,39]:

$$\sigma_{dB} \approx \sqrt{43\log\left(1+\left[\left(1+\frac{3}{\pi M}\right)\left(1+\frac{N}{\pi M}\right)^{-1}\right]\right)} \tag{16}$$

5.2. Sound insulation

The sound insulation of nine cross-laminated timber plates (CLT) from five different manufacturers were measured in the various transmission suites of two different acoustic laboratories. The surface area of the transmission suites varied; however, all plates had a measured area >10.6 m^2. The plates were of different thicknesses, consisted of either three or five layers and were installed in horizontal or vertical transmission suites. The effect of assembly variation on the calculated elastic moduli is shown in Tables 1 and 2. The sound insulation of the plates were measured in accredited facilities in accordance with EN ISO 10140 [11], and the reverberant test rooms aim to provide a standardised diffuse sound field incident on the partition. The pressure levels in the source and receiving rooms are measured, and losses due to absorption in the receiving room are quantified by measuring the reverberation times. Flanking transmission is also excluded using appropriate resilient elements, and flanking walls are shielded to ensure that the sound insulation of only the direct transmission is measured. This enables calculation of the sound insulation in third octave bands according to [11]:

$$R = L_{P,1} - L_{P,2} + 10\log\left(\frac{S}{A}\right) \tag{17}$$

where $L_{P,1}$ and $L_{P,2}$ are the sound pressure level in the source and receiver rooms, S is the area of the partition, and A is the absorption

area calculated from the reverberation time. (A = 0.161 V/T where T is the reverberation time and V is the volume of the receiving room.) The areas of the plates ranged from 10.6 m^2 to 12.0 m^2.

6. Results

6.1. Loss factor

The measured loss factors for plate 1 are compared with the calculated radiation loss factors for a baffled, unbaffled, and orthotropic thin plate in Fig. 3. The critical frequencies (f_c, f_{c1}, and f_{c2}) are calculated for this plate (according to appendix G) and these are used to determine the radiation efficiencies. The calculated radiation efficiency, and therefore the radiation loss factors, are increased when the edge conditions are more constrained. The radiation losses between the critical frequencies calculated using the infinite orthotropic thin plate model are the lowest within this frequency range (160–250 Hz), and the clamped edge perpendicularly baffled radiation losses could be considered a worst-case scenario. To ensure that the radiation coupling did not influence the measured loss factor, the estimated internal loss factor for plate 1 was calculated by averaging the measured loss factors in the third octave bands, which were shown to be significantly higher (>10 dB) than the maximum possible calculated radiation coupling. This is the solid line in Fig. 3. This measured value ($\eta_{measured}$ = 0.0218) was, however, found to be higher than values quoted in the literature for wood products. The implementation of this value in the thin plate orthotropic sound insulation model for plate 1 is presented in Fig. 4. An increased loss factor increases the calculated sound insulation above the critical frequency ($f > f_{c2}$). Therefore in all other cases, and to calculate the total percentage error of all the models, internal loss factors taken from the literature (η_{min} = 0.01, η_{max} = 0.016) [39] were preferred.

The calculated first mode ($f_{1,1}$) for the freely (FF-FF-FF-FF) supported and simply (SS-SS-SS-SS) supported plates are shown in Table 5. Measured values for plate 1 when freely supported and when installed for testing in the transmission suite are also shown. It is often assumed in sound insulation calculations that the plate boundary conditions are simply supported. In this case, the first modal frequency, when installed in the transmission suite (laboratory) is within 2.3 Hz of the calculated value for the same plate with simply supported boundary conditions, although this may not be similar to the actual boundary conditions in a real building. As shown in Table 5 different boundary conditions can radically change the frequency of the principal mode (and subsequent modes), hence actual modal densities (at low frequencies < 250 Hz). Rindel [17] advises that statistical methods are suitable for prediction at frequencies higher than the first mode of the plate (preferably $f > 4f_{1,1}$). The third octave band building acoustics range for which this condition is fulfilled is also indicated in Table 5. Two ranges are indicated for plate 9 corresponding to the two different plate sizes.

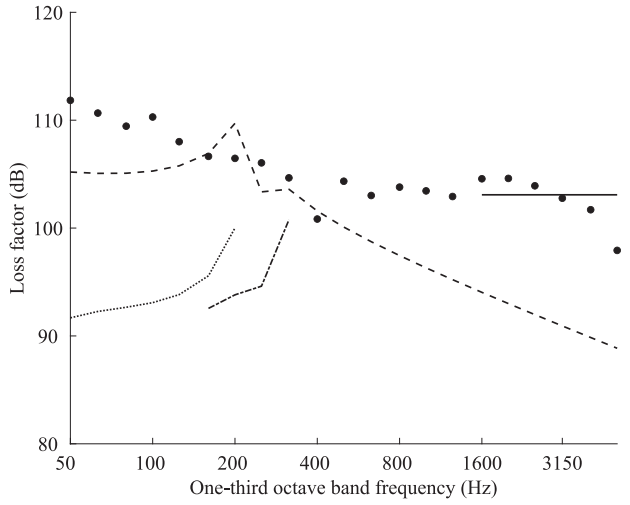

Fig. 3. '●' Measured loss factor, impulse decay using a large hammer and T_5 compared to the calculated radiation losses. '-' The solid line denotes the values used to determine the measured internal loss factor, '–' the dashed line denotes the maximum (baffled) radiation losses, '-.' the dash dot line denotes the minimum (orthotropic) radiation losses ($f_{c1} < f < f_{c2}$) and '. . .' the dotted line indicates the unbaffled radiation losses. ($f < f_c$).

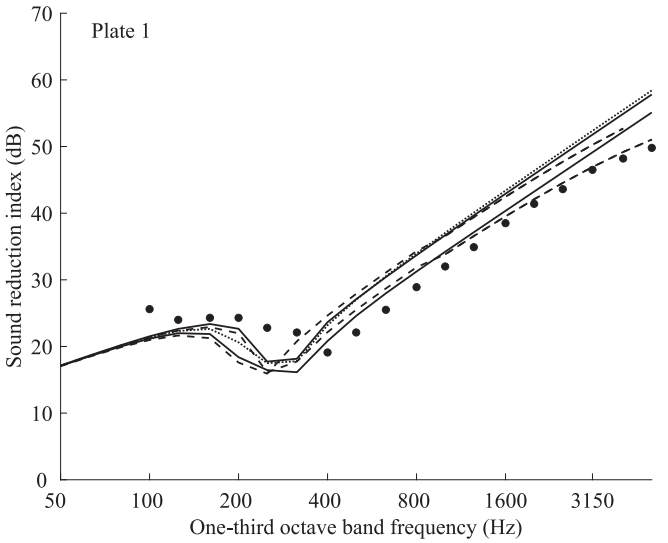

Fig. 4. '●' Measured vs modelled sound insulation comparison of the two models, ρ = 438kgm^{-3}. '-' Solid lines denote the upper and lower limits of the orthotropic thin plate model, '–' dashed lines denote the upper and lower limits of the isotropic thick plate model and '. . .' the dotted line indicates the calculated values using the measured loss factor.

The modal overlap factor, M, for the freely (FF-FF-FF-FF) and simply (SS-SS-SS-SS) supported plates are presented in Tables 6 and 7 for low frequencies (50–250 Hz). These values are similar, within this frequency range, to typical statistical values for heavyweight materials such as concrete (0.1–0.5) masonry (0.1–0.8) or solid dense aggregate blocks (0.04–0.2) [39]. The uncertainty of structural measurements such as velocity levels or coupling loss factors are increased when modal overlap factors are less than one, or there are less than five modes per third octave band [39]. Third octave bands with less than five modes are shown in brackets; for many of the low frequency bands, both criteria are not met. Low modal overlap factors would not be expected to significantly influence the uncertainty of airborne sound transmission; the modal overlap of the receiving room is usually of more relevance [11,46]. However, sound radiation models based on the radiation of individual modes [47] rather than a statistical modal count [44] may produce more accurate models at low frequencies (<250 Hz).

The measured loss factor of the freely supported plate is high. Higher damping results in broader modes (i.e., with an increased Q-factor) and increased modal overlap factors. The measured loss factor was therefore used to calculate the modal overlap factors of the CLT plate in a best-case scenario. The modal overlap factors and mode count were also used to determine the expected standard deviations of velocity levels or structure-borne coupling loss factors of the nine plates. These expected standard deviations in structure-borne applications for the simply supported plate are shown in Table 8; all standard deviations >3.6 dB are listed.

Table 5
First modal frequency of the freely supported (FF-FF-FF-FF) and simply supported (SS-SS-SS-SS) plates.

	FF-FF-FF-FF	FF-FF-FF-FF (measured)	SS-SS-SS-SS	Installed in the laboratory (measured)	Third octave band range for which (SS-SS-SS-SS) $f > 4f_{1,1}$
	$f_{1,1}$ (Hz)	$f_{1,1}$ (Hz)	$f_{1,1}$ (Hz)	$f_{1,1}$ (Hz)	(Hz)
Plate 1	8.7	8.2	22.3	20.0	100–5000
Plate 2	10.0	–	24.7	–	125–5000
Plate 3	13.0	–	32.8	–	160–5000
Plate 4	17.8	–	43.6	–	200–5000
Plate 5	21.9	–	52.4	–	250–5000
Plate 6	12.6	–	22.2	–	100–5000
Plate 7	9.4	–	18.1	–	100–5000
Plate 8	8.0	–	19.0	–	100–5000
Plate 9	[2]6.7/13.9	–	[2]16.9/34.7	–	[2]160-5000/80–5000

[2] Two aspect ratios were used.

Table 6
Calculated maximum modal overlap factors in the 50–250 Hz third octave bands for freely supported plates (FF-FF-FF-FF). Modal overlap factors calculated from < 5 modes per third octave band are shown in brackets.

M (-)	50 Hz	63 Hz	80 Hz	100 Hz	125 Hz	160 Hz	200 Hz	250 Hz
Plate 1	(0.177)	(0.176)	(0.178)	(0.089)	(0.438)	(0.352)	(0.265)	0.701
Plate 2	(0.265)	(0.176)	(0.178)	(0.0)	(0.438)	(0.352)	(0.265)	(0.526)
Plate 3	(0.088)	(0.176)	(0.267)	(0.089)	(0.175)	(0.176)	(0.442)	(0.438)
Plate 4	(0.0)	(0.088)	(0.178)	(0.089)	(0.175)	(0.176)	(0.088)	(0.438)
Plate 5	(0.0)	(0.088)	(0.0)	(0.266)	(0.088)	(0.088)	(0.177)	(0.175)
Plate 6	(0.0)	(0.263)	(0.0)	(0.266)	(0.263)	(0.176)	(0.531)	(0.175)
Plate 7	(0.265)	(0.0)	(0.267)	(0.266)	(0.175)	(0.440)	(0.442)	(0.351)
Plate 8	(0.177)	(0.0)	(0.178)	(0.266)	(0.351)	(0.264)	0.619	(0.263)
Plate 9	(0.177)	(0.176)	(0.178)	(0.533)	(0.351)	(0.264)	0.884	(0.526)

Table 7
Calculated maximum modal overlap factors in the 50–250 Hz third octave bands for simply supported plates (SS-SS-SS-SS). Modal overlap factors calculated from < 5 modes per third octave band are shown in brackets.

M (-)	50 Hz	63 Hz	80 Hz	100 Hz	125 Hz	160 Hz	200 Hz	250 Hz
Plate 1	(0.0)	(0.088)	(0.178)	(0.178)	(0.088)	(0.088)	(0.531)	(0.175)
Plate 2	(0.0)	(0.088)	(0.0)	(0.266)	(0.088)	(0.176)	(0.442)	(0.175)
Plate 3	(0.088)	(0.0)	(0.089)	(0.089)	(0.175)	(0.176)	(0.177)	(0.263)
Plate 4	(0.0)	(0.088)	(0.0)	(0.0)	(0.088)	(0.176)	(0.177)	(0.088)
Plate 5	(0.088)	(0.0)	(0.0)	(0.089)	(0.0)	(0.088)	(0.177)	(0.088)
Plate 6	(0.088)	(0.088)	(0.089)	(0.089)	(0.088)	(0.264)	(0.177)	(0.438)
Plate 7	(0.0)	(0.088)	(0.178)	(0.089)	(0.263)	(0.176)	(0.354)	(0.351)
Plate 8	(0.0)	(0.176)	(0.089)	(0.089)	(0.088)	(0.440)	(0.177)	(0.526)
Plate 9	(0.0)	(0.263)	(0.178)	(0.089)	(0.263)	(0.440)	(0.354)	0.614

Table 8
Calculated standard deviations of velocity level measurements and/or structural coupling factors in third octave bands for simply supported plates (SS-SS-SS-SS) in structure-borne applications.

s.d. (dB)	50 Hz	63 Hz	80 Hz	100 Hz	125 Hz	160 Hz	200 Hz	250 Hz	315 Hz	>400 Hz
Plate 1	3.8	3.7	3.7	3.7	3.7	3.7	3.4	3.7	3.4	<3.6
Plate 2	3.9	3.8	3.9	3.6	3.8	3.7	3.4	3.7	3.4	<3.6
Plate 3	3.8	3.9	3.8	3.8	3.7	3.7	3.7	3.6	3.4	<3.6
Plate 4	3.9	3.8	3.9	3.9	3.8	3.7	3.7	3.8	3.7	<3.6
Plate 5	3.8	3.9	3.9	3.8	3.9	3.8	3.7	3.8	3.8	<3.6
Plate 6	3.7	3.7	3.7	3.7	3.7	3.6	3.7	3.5	3.6	<3.6
Plate 7	3.8	3.7	3.6	3.7	3.6	3.6	3.5	3.5	3.5	<3.6
Plate 8	3.8	3.7	3.7	3.7	3.7	3.5	3.7	3.4	3.5	<3.6
Plate 9	3.8	3.6	3.7	3.7	3.6	3.5	3.5	3.3	3.3	<3.6

6.2. Sound insulation

The measured and predicted values of sound reduction index for plate 1 are presented in Fig. 4. Upper and lower limits are defined by the equivalent elastic moduli including the fifth percentile of the elastic modulus in the direction parallel to the grain ($E_{eq,x} \pm \Delta E_{eq,x,0.05}$ and $E_{eq,x} \pm \Delta E_{eq,y,0.05}$) and the internal loss factor η_{min} = 0.01 and η_{max} = 0.016 taken from the literature [39]. The sound insulation determined from the elastic modulus ($E_{eq,x}$) and the measured loss factor is also shown. As described in section 5.1 the measured loss factor is somewhat overestimated compared with those quoted in the literature for wood products and this results in an increased calculated sound insulation. The measured single figure values are $R_w(C;C_{tr})$ = 30(-1;-3) and the predicted single figure values are $R_w(C;C_{tr})$ = 30(-1;-4) for the mean of the orthotropic thin plate model limits and $R_w(C;C_{tr})$ = 31(-1;-5) for the mean of the isotropic thick plate model limits. All single number ratings are calculated according to EN ISO 717 [48]. For the

Table 9
The combined influence of the fifth percentile of the elastic modulus and the loss factor for plates 1, 3, and 6–9.

Plate	Manufacturer	% of measured values within the calculated thin plate range
1	A	0.0
3	B	19.0
6	C	42.9
7	D	19.0
8	D	19.0
9	E	38.1
Overall	–	23.6

thick plate model, poor agreement between measured and predicted single figure values at low frequencies (<1000 Hz) (see also Table 10) is due to the assumption of isotropy. The main difference between the orthotropic and isotropic models is in the low frequency region; the orthotropic model has two troughs due to two separate critical frequencies (see Figs. 1 and 4) and the isotropic model has one (Fig. 4). The orthotropic thin plate model is more accurate at low frequencies (<1000 Hz), for this reason and for clear presentation of the sound insulation accuracy, data for the thick plate model are not displayed in Fig. 5 below this cut-off frequency. Above the critical frequencies (f_c, f_{c1}, and f_{c2}) an isotropic thin plate model, compared to an orthotropic thin plate model, would be expected to increase the sound insulation by no more than + 0.5 dB.

The percentage differences in the equivalent elastic moduli due to the different calculation methods are shown in Table 2. The equivalent elastic moduli using modified gamma theory are somewhat reduced in the y-direction only. Equivalent elastic moduli reduced by <18.6 % in the orthotropic thin plate model result in deviations in the third octave band sound insulation of <1.0 dB. The larger the plate, the lower the influence of this correction. The fifth percentile of the elastic modulus in the direction parallel to the grain has a much greater influence on the equivalent elastic moduli with differences of up to 46.9 % in the x-direction and up to 51.0 % in the y-direction. The combined influence of the fifth percentile of the elastic modulus and the loss factor can be isolated for plates 1, 3, and 6–9 where the density of the plates were recorded in the laboratory. Table 9 shows the accuracy of the prediction in these cases.

Examining the data for plate 1 more closely, the influence of the fifth percentile of the elastic modulus in the direction parallel to the grain on the equivalent elastic moduli is 16.3 % in the x-direction and 17.8 % in the y-direction. The combined influence of the elastic modulus and the loss factor on the third octave band sound insulation calculated for plate 1 are indicated in Fig. 4. Deviations of up to ± 2.1 dB are observed for the orthotropic thin plate model, however, 0 % of the measured values fall within this calculated range. To help identify the underlying reasons for this, more information about the panel density, such as the fifth percentile of the density of the panel material, should be provided in the literature and standards concerning CLT.

The predicted results are compared with measurements for plates 2 to 9 in Fig. 5. Three- and five-layer panels are distinguished by using open and closed circles in the diagrams; error bars are shown for panels where more than one test result was available. The combined influences of the fifth percentile of the elastic modulus in the direction parallel to the grain, the surface density, and the loss factor on the third octave band sound insulation on the orthotropic thin plate model are indicated. The relationships between surface density and the surface impedance, Z, (see appendix B) which is used to determine the sound insulation are different in the frequency ranges above ($f > f_{c2}$) and below ($f < f_{c1}$) the critical frequencies; therefore, the low frequency limits are determined by different combinations of the maximum and minimum variables. The limits for sound insulation at low frequencies are calculated using the $R_{min}(B_{min}, \rho_{s,min}, \eta_{min})$ or $R_{max}(B_{max}, \rho_{s,max}, \eta_{max})$ combinations and at high frequencies using $R_{min}(B_{min}, \rho_{s,max}, \eta_{min})$ or $R_{max}(B_{max}, \rho_{s,min}, \eta_{max})$ combinations respectively. The two sets of limits are separated in Fig. 5 by a gap.

The overall accuracy of the models was determined by the percentage of points which fall within the upper and lower modelled limits. This is 44.0 % of measured results (50–5000 Hz) when compared with the orthotropic thin plate model and 57.0 % of the measured results (50–5000 Hz) when compared with the isotropic thick plate model. Closeness of fit regarding the prediction of the single figure sound reduction index values are shown in Table 10; in the case of multiple measurements, the mode of these values is displayed. These are calculated according to:

$$\Delta R_W = R_{W,meas} - R_{W,calc} \tag{18}$$

The orthotropic thin plate model consistently underestimates the single figure sound insulation of the plates (i.e., seven of the nine cases). The isotropic thick plate model also underestimates the single figure sound insulation in six of the nine cases. The thinnest plate, plate 3, shows the poorest agreement (in R_W) between the models and measurement.

The low frequencies show the poorest agreement with calculated results for plates 1, 2, 3, 4, 5, and 7. Three of the three-layer panels and three of the five-layer panels exhibit significantly higher than expected sound insulation at low frequencies (<500 Hz); this is the part of the sound insulation curve governed by the mass. As a perfectly diffuse field is difficult to achieve even under laboratory conditions, discrepancies between model and measurement may be caused by a non-diffuse field on the panel or in the receiving room at low frequencies ($f < f_{c1}$). Another possible cause is if excessive flanking transmission is directed away from the receiving room and excluded from the laboratory, which would result in an artificially increased sound insulation measurement. Without further information about the exact laboratory conditions in each case, far beyond the details provided by the standard measurement conditions, it is difficult to appropriately adjust the modelling conditions to obtain better agreement. The sound field in the room [49], structure-borne sound field [50] and boundary conditions [44,45] of the plate also affect the applicability of sound insulation measurements to existing buildings. In all infinite plate models, the angles of incident sound were assumed to be perfectly diffuse, with all angles of incidence of equal probability. The effect of weighting the angle distribution using field incidence, an alternative distribution [41,51], or spatial windowing [52–54] to account for the finite size of the plate was not considered here, these modifications can increase the sound insulation (f_c, f_{c1}, and f_{c2}) and could be considered in further work. However, prominent peaks and troughs in the sound insulation at low frequencies could indicate dominant modal behaviour rather

Table 10
Closeness of fit for the mean of the upper and lower limits of the models to single figure values $R_w(C;C_{tr})$.

Model	Orthotropic thin plate			Isotropic thick plate		
	ΔR_w	ΔC	ΔC_{tr}	ΔR_W	ΔC	ΔC_{tr}
Plate 1	0	0	1	−1	0	2
Plate 2	3	0	1	3	0	1
Plate 3	6	0	0	5	0	1
Plate 4	3	0	3	2	1	3
Plate 5	4	1	3	4	1	3
Plate 6	2	0	1	1	1	2
Plate 7	3	0	1	2	0	2
Plate 8	0	2	2	−1	2	3
Plate 9	1	0	0	0	1	1

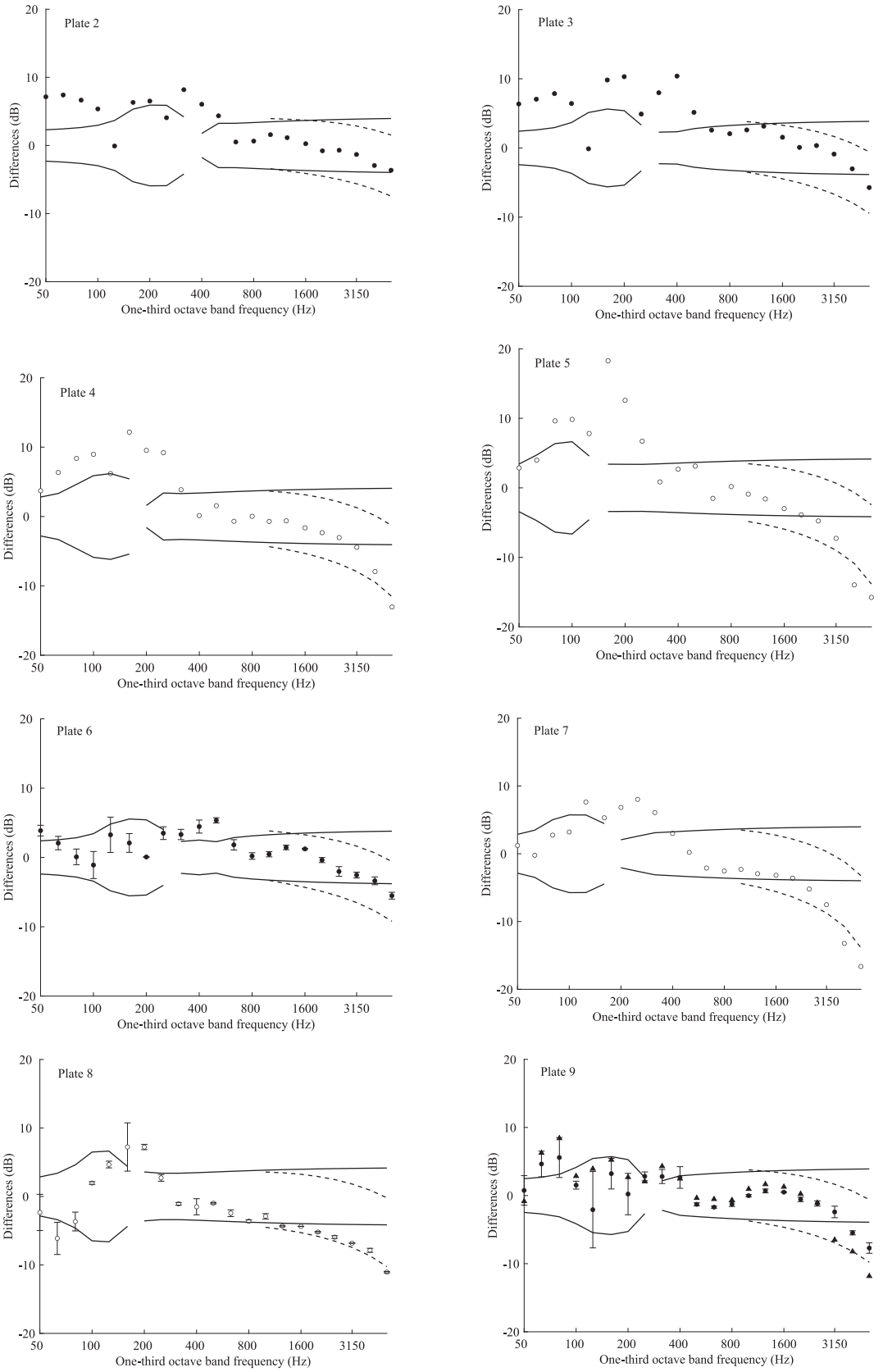

Fig. 5. Accuracy of the two models to predict sound insulation; all data is normalised to the orthotropic thin plate model. '-' Solid lines denote the upper and lower limits of the orthotropic thin plate model, '–' dashed lines denote the upper and lower limits of the isotropic thick plate model (1 kHz to 5 kHz only). Measured data is indicated by: 'o' open circles denote five-layer CLT, '●' closed circles denote three-layer CLT, '▲' triangles denote a plate with identical plate cross section with lower aspect ratios (L_x/h and L_y/h). Where multiple measurements were made, 95 % confidence limits are shown. (Note that the use of an orthotropic thick plate model, but an isotropic thick plate model offsets the thick plate model curve in these diagrams by no more than + 0.5 dB.).

than diffuse field behaviour [50], which may account for disagreement between the model and measurement at low frequencies. These peaks and troughs would also affect the single figure sound insulation (R_w) ratings. Finally, common methods used to suppress flanking transmission in the laboratories include shielding of the walls, floor, and ceiling, and this may have the side effect of channelling power away from the receiving room in the measurement, thus increasing measured sound insulation.

All but one of the panels (plate 1) were anonymised, and therefore different manufacturing methods are not identifiable and were not considered. The orthotropic thin plate theory used to determine the sound insulation was poor at correctly predicting the low frequency performance. More information about the panel assembly procedures such as edge bonding, gaps and stress relief cuts (in the core layer), workmanship, and product types such as solid wood panels (MSWP) may be required. However, precision information about the test conditions is more likely to be the primary factor required to determine the exact causes. Three of the five-layer panels clearly have plateaus in the sound insulation at high frequencies (>2000 Hz), which exceed that predicted by the isotropic thick plate theory. This trend can also be observed in the measured three-layer plate results marked by solid triangles (▲). This suggests an increased shear deformation effect of the core layers; however, it is difficult to identify a specific trend. The thin plate limit given by Eq. (8) is limited in applicability; the plateau in sound insulation also depends on the aspect ratio (h/b) as evidenced in the high frequency range (f > 2500 Hz) by plate 9, where two aspect ratios were measured. As an additional complication, CLT plates with three (and potentially more) layers could also be described as having semi-thick behaviour, which exhibit plateaus in the dispersion relation at different frequencies in different material directions. The elastic constants of the plate (E_x and E_y) can be adjusted to model this behaviour using an empirical method; however, it is preferable if these constants are also accounted in the modal performance of the plate at low frequencies. Such an approach which combines orthotropic and thick plate effects to calculate sound insulation could improve the predicted sound insulation of CLT plates.

7. Conclusion

Radiation losses may affect the measurement of internal loss factors of CLT plates. Lightweight materials often have high internal loss factors that may be obscured in certain frequency bands by radiation losses, making them difficult to measure. Even when the radiation coupling losses were considered, the measured internal losses were overestimated when the plate was freely hanging in the laboratory. The first mode for freely supported (FF-FF-FF-FF) and simply supported (SS-SS-SS-SS) plates is in each case below the frequency range of interest for acoustic applications (50–5000 Hz). However, low mode counts, and consequently low modal overlap, will result in uncertainties in structural measurements. In the case of direct airborne transmission only for such plates, sound radiation models based on the radiation coupling of individual modes may be more appropriate at low frequencies (<250 Hz) than an infinite plate or statistical energy description.

The modified gamma theory applied as described, results in an equivalent elastic modulus in the y-direction that was modified by no more than 18.6 %, which changes the modelled sound insulation of an infinite thin orthotropic plate by up to 1.0 dB. Accounting for the fifth percentile of the elastic modulus in the direction parallel to the grain produces significantly greater differences in the moduli in both the x- and y- material directions. This together with the described upper and lower limits on the density and internal loss factor results in broad upper and lower limits on calculated sound insulation. The precision of orthotropic thin plate and isotropic thick plate models to predict R is in the worst case ± 6.6 dB (panels 5 & 8, Fig. 5). Simply determining the exact density of the individual panel (as shown in the measurement of panel 1) can significantly narrow this range (±1.6 dB, Fig. 4). However, it is recommended that more information about the panel density, such as the fifth percentile of the density of the panel, be provided in future literature and standards concerning CLT. Without additional information from the manufacturer about the density distribution in the panel, a prediction based on the recorded density from a single panel, such as typically measured during a sound insulation test, fails to determine the sound insulation behaviour, particularly at low frequencies (f > 250 Hz). A model which accounts for dominant modal behaviour in this frequency range could also improve predictions. A combined orthotropic and thick plate sound insulation model may also be required to improve the predicted sound insulation of CLT plates at high frequencies ($f \geq$ 1000 Hz). In some cases, such as in the case of plate 1, the behaviour could be described as semi-thick, exhibiting plateaus in the dispersion relation at different frequencies in different material directions.

Data availability

The authors do not have permission to share data.

Declaration of Competing Interest

The authors declare the following financial interests/personal relationships which may be considered as potential competing interests: Two of the authors are employed by Holzforschung Austria (HFA) which is a research and development organisation, carrying out testing and monitoring, and providing laboratory certification and calibration for wood products. The research did not receive any specific grant from funding agencies in the public, commercial, or not-for-profit sectors. HFA provided data for eight of the plates to validate the models. The loss factor measurements and sound insulation of one plate were carried out at the Swiss Federal Laboratories for Materials Science and Technology (EMPA); this CLT plate was provided by Schuler AG. Some data analysis was also carried out by Dr Mathew Robinson thanks to the collaboration of the University of Liverpool. Aside from this the authors declare that they have no known competing financial interests or personal relationships that could have appeared to influence the work reported in this paper.

Acknowledgements

This research did not receive any specific grant from funding agencies in the public, commercial, or not-for-profit sectors. Thanks to Holzforschung Austria (HFA) for providing data for plates 2 to 9 to validate the models; this data has been anonymised for publication. The loss factor measurements and sound insulation of plate 1 were carried out at the Swiss Federal Laboratories for Materials Science and Technology (EMPA); this CLT plate was provided by Schuler AG. The support of these companies and laboratories is gratefully acknowledged. Thanks also to Dr Mathew Robinson for carrying out the analysis of recorded impulse responses of the CLT plate to obtain the loss factor from a T_5 measurement. Thank you to Dr Elaine Massung of Blue Eagle Academic Services (https://academic-smartcuts.com/) for proofreading, Dr Rebecca Ghent for technical proofreading of the paper and Prof Trevor Cox for his recommendations concerning the title, abstract and introduction. The authors acknowledge the TU Wien Bibliothek for financial support through its Open Access Funding Program.

Appendix A. Gamma factor, γ_i, to account for shear deflection of bonded core layers

The proposed modifying factors, γ_i, are to account for shear deflection of bonded core layers rather than mechanical slippage. The outer layers for plates with three or five layers in the x- and y- directions are given by [15]:

$$\gamma_{i,x} = \begin{cases} \left(1 + \frac{\pi^2 E_i h_i}{L_{\text{eff}}^2 (G_{yz}/h_j)}\right)^{-1} & i = 1,5 \text{ (or } 1,3) \\ 1 & i = 2,3,4 \text{ (or } 2) \end{cases} \tag{A1}$$

$$\gamma_{i,y} = \begin{cases} \left(1 + \frac{\pi^2 E_i h_i}{L_{\text{eff}}^2 (G_{xz}/h_j)}\right)^{-1} & i = 1,5 \text{ (or } 1,3) \\ 1 & i = 2,3,4 \text{ (or } 2) \end{cases} \tag{A2}$$

where L_{eff} is the effective length of the beam (e.g., the width, L_x, or length, L_y, of the plate, assuming support at the end points), G_{xz} or G_{yz} is the appropriate shear modulus considering the material directions of the layers, and j is the layer connecting the ith layer to the middle plate layer.

Appendix B. The surface impedance of a thin plate

The surface impedance of a thin plate is given by [41,42]:

$$Z = i\omega\rho_s \left[1 - \left(\frac{B_{p,x}\cos^2\phi}{\omega^2\rho_s} + \frac{B_{p,y}\sin^2\phi}{\omega^2\rho_s}\right)^2 k^4 \sin^4\theta\right] \tag{B1}$$

The bending stiffness of the material is calculated from the equivalent elastic moduli $B_x = E_{eq,x}h^3/(12(1-\nu_{xy}\nu_{yx}))$ and $B_y = E_{eq,y}h^3/(12(1-\nu_{xy}\nu_{yx}))$. The estimated internal loss factor, η, is used to determine the complex bending stiffnesses $B_{p,x} = B_x(1 + i\eta)$, and $B_{p,y} = B_y(1 + i\eta)$. The values of the internal loss factor implemented in this calculation are described in section 5.1. In an isotropic model the following bending stiffness is substituted for the plate bending stiffnesses in the x- and y- directions in Eq. (B.1).

$$B_{\text{iso}} = \sqrt{B_x B_y} \tag{B2}$$

where $B_x = E_x h^3/12(1\text{-}\nu^2)$ and $B_y = E_y h^3/12(1\text{-}\nu^2)$.

Appendix C. The thick plate correction term

The thick plate correction term based on Ljunggren [43]:

$$\Delta R_c = 10\lg(A/BC) \tag{C1}$$

$$A = [1 + (h^2/12)\left(\frac{k_c^2 k_S^2}{k_L^2} - k_S^2\right)]^2 \tag{C2}$$

$$B = 1 - \frac{(k_S h)^2}{12} + \frac{k_c^2\left(k_S^2 + k_L^2\right)}{k_B^4} \tag{C3}$$

$$C = [1 - \frac{(k_S h)^2}{12} + \left(k_S^2 + k_L^2\right)^2/(4k_B^4)]^{1/2} \tag{C4}$$

where k_L is the quasi-longitudinal wavenumber, k_S is the wave number of a hypothetical Rayleigh wave, and k_c is the wavenumber at coincidence. The quasi-longitudinal wavenumber can be obtained from:

$$k_L = \omega\sqrt{\frac{\rho h^3}{12B_{iso}}} \tag{C5}$$

The Rayleigh wavenumber (referred to as a corrected shear wave in [43]) can be obtained from

$$k_S = \omega\sqrt{\frac{\rho}{\kappa^2 G_{iso}}} = \frac{\omega}{\kappa}\sqrt{\frac{2(1+\nu)\rho}{E_{iso}}} \tag{C6}$$

There are several possible ways to determine the wavenumber at coincidence. The method used in this research is to rearrange the equation for the modified phase velocities based on Mindlin [55]; this is similar to Cremer et al. [14] but retains the shear correction factor, κ:

$$k_{B,\text{thick}}^4 - k_{B,\text{thick}}^2\omega^2\left[\frac{1}{\kappa^2 c_S^2} + \frac{1}{c_L^2}\right] + \frac{\omega^4}{c_L^2\kappa^2 c_S^2} - k_{B,p}^4 = 0 \tag{C7}$$

where $c_L = c_{L,p}$ in Eq. (9) and

$$c_S = \sqrt{\frac{G_{iso}}{\rho}} \tag{C8}$$

then setting the phase velocity equal to the speed of sound in air ($c_{B,\text{thick},p} = c_0 = 343\ \text{ms}^{-1}$) and solving for the wavenumber using MATLAB. To simplify this equation, the shear correction factor may be assumed to equal one ($\kappa = 1$). However, Ljunggren [43] recommends that the shear correction factor (κ) given by Magrab [56] be used

$$\kappa \approx \frac{(0.87 + 1.12\nu)}{(1+\nu)} \tag{C9}$$

where ν is the isotropic Poisson's ratio.

Appendix D. The radiation efficiency of a finite baffled plate (with simply supported and clamped conditions)

The radiation efficiency of a baffled plate is given by [44]:

$$\sigma = \begin{cases} \frac{U}{2\pi\mu k S\sqrt{\mu^2-1}}\left[\ln\left(\frac{\mu+1}{\mu-1}\right) + \frac{2\mu}{\mu^2-1}\right]\left[C_{BC}C_{OB} - \mu^{-8}(C_{BC}C_{OB} - 1)\right] & (f < f_c) \\ \left(0.5 - \frac{0.15L_1}{L_2}\right)\sqrt{k}\sqrt{L_1} & (f = f_c) \\ \frac{1}{\sqrt{1-\mu^2}} & (f > f_c) \end{cases} \tag{D1}$$

where $\mu = \sqrt{f_c/f}$, U is the plate perimeter, S is the plate area, C_{BC} is a constant for the plate boundary conditions ($C_{BC} = 1$ for simply supported boundaries, $C_{BC} = 2$ for clamped boundaries), C_{OB} is a constant for the orientation of the baffle that surrounds the edges of the plate ($C_{OB} = 1$ when the plate lies within the plane of an infinite rigid baffle, $C_{OB} = 2$ when the rigid baffles along the plate perimeter are perpendicular to the plate surface), and L_1 is the smaller and L_2 is the larger of the rectangular plate dimensions, L_x and L_y (for square plates, $L_1 = L_2 = L_x = L_y$). The radiation efficiency for the frequency band that contains the critical frequency in Eq. (11) (or Eq. (D.1)) can be calculated using $k = 2\pi f_c/c_0$, where f_c is the critical frequency of the plate (see appendix G) and c_0 is the speed of sound in air.

Appendix E. Radiation efficiency at the edges and corners of a rectangular plate

The radiation efficiency at the corners of the plate is given by [45]

$$\sigma_{corner} = \frac{2r_s}{\pi^4}\left(\frac{\lambda_c^2}{S}\right) \times \begin{cases} \left(1 - \frac{2}{\mu^2}\right)/\frac{1}{\mu}\left(1 - \frac{1}{\mu^2}\right)^{1/2} & (f < f_c/2) \\ 0 & (f \geq f_c/2) \end{cases} \tag{E1}$$

where r_s is the number of corners. See appendix G for a calculation of the critical frequency, f_c of the plate. The radiation efficiency at the edges of the plate is given by [45]:

$$\sigma_{edge} = \frac{1}{4\pi^2}\left(\frac{U\lambda_c}{S}\right)\left[\frac{\left(1-\frac{1}{\mu^2}\right)\ln\left(\frac{\left(1+\frac{1}{\mu}\right)}{\left(1-\frac{1}{\mu}\right)}\right)+\frac{2}{\mu}}{\left(1-\frac{1}{\mu^2}\right)^{3/2}}\right] \quad \text{(E2)}$$

Appendix F. Correction factors due to the interaction between the power flows on each side and around the perimeter of the plate

The correction factors due to the interaction between the power flows on each side and around the perimeter of the plate are given by [45]:

$$F_{plate} = 53f^4S^2/c_0^4(1+53f^4S^2/c_0^4)^{-1} \quad \text{(F1)}$$

$$F_{corner} = \frac{1}{2}[13/\mu^2(1+13/\mu^2)^{-1}] \quad \text{(F2)}$$

$$F_{edge} = \frac{1}{2}[49/\mu^2(1+49/\mu^2)^{-1}] \quad \text{(F3)}$$

Appendix G. Critical frequency

In the isotropic case the critical frequency is given by [39]:

$$f_c = \frac{c_0^2}{2\pi}\sqrt{\frac{\rho h}{B_x B_y}} \quad \text{(G1)}$$

In the orthotropic case the critical frequencies are given by [42]:

$$f_{c,i} = \frac{c_0^2}{2\pi}\sqrt{\frac{\rho h}{B_i}} \quad \text{(G2)}$$

where i = 1 or 2, $f_{c,1}$ is given by $B_i = \max(B_x, B_y)$ and $f_{c,2}$ is given by $B_2 = \min(B_x, B_y)$.

References

[1] Amiri A, Ottelin J, Sorvari J, Junnila S. Cities as carbon sinks—classification of wooden buildings. Environ Res Lett 2020;15(9):094076.
[2] Lan K, Kelley SS, Nepal P, Yao Y. Dynamic life cycle carbon and energy analysis for cross-laminated timber in the Southeastern United States. Environ Res Lett 2020;15(12):124036.
[3] Ortiz O, Castells F, Sonnemann G. Sustainability in the construction industry: A review of recent developments based on LCA. Constr Build Mater 2009;23 (1):28–39.
[4] Monte Rosa Hut. Motion Picture. Switzerland: Copyright Holcim AG; 2015.
[5] Kübler W. Freiformschale Elefantpark Zoo Zürich: Statische Formfindung und Konstruktion. [Conference presentation]. In: Proceedings of Holzbautag.Biel, Switzerland, 2013.
[6] Anteman M. The Tamedia building Zurich. In: Proceedings of Wood Build 2013. Oslo, Norway., 2013.
[7] Borgström E, Fröbel J. The CLT Handbook - CLT structures - facts and planning. Stockholm: Swedish Wood; 2019.
[8] EN 1995-1-1 Eurocode 5: Design of timber structures - Part 1-1: General - Common rules and rules for buildings. 2004+A1(2006).
[9] EN 338 Structural timber - strength classes. European Committee for Standardization (CEN); 2003.
[10] Bodig J, Jayne B. Mechanics of Wood and Wood Composites. Reprint with corrections ed:. Florida: Krieger publishing company; 1993.
[11] EN ISO 10140-1 Acoustics — Laboratory measurement of sound insulation of building elements, Part 1: Application rules for specific products. CEN, ISO; 2016.
[12] EN ISO 10848 Acoustics — Laboratory measurement of the flanking transmission of airborne and impact sound between adjoining rooms. CEN, ISO; 2006.
[13] EN 12354-1 Building acoustics — Estimation of acoustic performance of buildings from the performance of elements — Part 1: Airborne sound insulation between rooms. CEN; 2000.
[14] Cremer L, Heckl M, Pederson BAT. Structure-Borne Sound. Third ed:. Berlin Heidelberg New York: Springer; 2005.
[15] Navaratnam S, Christopher PB, Ngo T, Le TV. Bending and shear performance of Australian Radiata pine cross-laminated timber. Constr Build Mater 2020;232:117215.
[16] Stürzenbecher R, Hofstetter K, Eberhardsteiner J. Structural design of Cross Laminated Timber (CLT) by advanced plate theories. Compos Sci Technol 2010;70(9):1368–79.
[17] Rindel JH. Dispersion and absorption of structure borne sound in acoustically thick plates. Appl Acoust 1994;41(2):97–111.
[18] Kurtze G, Watters BG. New wall design for high transmission loss or high damping. J Acoust Soc Am 1959;31(6):739–48.
[19] Wareing RR, Davy JL, Pearse JR. The sound insulation of single leaf finite size rectangular plywood panels with orthotropic frequency dependent bending stiffness. J Acoust Soc Am 2016;139(1):520–8.
[20] Lyon RH, DeJong RG. Chapter 8 Evaluating the mode count. Theory and applications of SEA. Newnes: Elsevier; 1994. p. 135–52.
[21] Moarcas O, Irle M. Determination of Poissons ratio for particleboard in pure bending. Wood Sci Technol 1999;33(5):439–44.
[22] Ozyhar T, Hering S, Niemz P. Moisture-dependent orthotropic tension-compression asymmetry of wood. Holzforschung 2013;67(4):395–404.
[23] Ozyhar T, Hering S, Niemz P. Viscoelastic characterization of wood: Time dependence of the orthotropic compliance in tension and compression. J Rheol 2013;57(2):699–717.
[24] Niemz P, Caduff D. Untersuchungen zur Bestimmung der Poissonschen Konstanten an FichtenholzResearch into determination of the Poisson ratio of spruce wood. Holz Roh Werkst 2008;66(1):1–4.
[25] Ozyhar T, Hering S, Sanabria SJ, Niemz P. Determining moisture-dependent elastic characteristics of beech wood by means of ultrasonic waves. Wood Sci Technol 2013;47(2):329–41.
[26] Zhou J, Chui YH, Gong M, Hu L. Elastic properties of full-size mass timber panels: Characterization using modal testing and comparison with model predictions. Compos B Eng 2017;112:203–12.
[27] Zhou J, Chui YH, Niederwestberg J, Gong M. Effective bending and shear stiffness of cross-laminated timber by modal testing: Method development and application. Composites Part B: Engineering; 2020. p. 198.
[28] Churchill C. Evaluating the dynamic elastic constants of a cross-laminated timber (CLT) plate for acoustic and vibroacoustic problems. (submitted 23/08/2021).
[29] Gülzow A, Richter K, Steiger R. Influence of wood moisture content on bending and shear stiffness of cross laminated timber panelsEinfluss der Holzfeuchte auf die Biege- und Schubsteifigkeit von Brettsperrholzplatten. Eur J Wood Wood Prod 2011;69(2):193–7.
[30] Waddington DC, Woodcock J, Peris E, Condie J, Sica G, Moorhouse AT, et al. Human response to vibration in residential environments. J Acoust Soc Am 2014;135(1):182–93.
[31] Hu LJ, Chui YH, Onysko DM. Vibration serviceability of timber floors in residential construction. Prog Struct Eng Mater 2001;3(3):228–37.
[32] Persson Waye K, Rylander R. The Prevalence of Annoyance and Effects after Long-Term Exposure to Low-Frequency Noise. J Sound Vib 2001;240 (3):483–97.
[33] Santoni A, Schoenwald S, Van Damme B, Fausti P. Determination of the elastic and stiffness characteristics of cross-laminated timber plates from flexural wave velocity measurements. J Sound Vib 2017;400:387–401.
[34] Damme BV, Schoenwald S, Zemp A. Modeling the bending vibration of cross-laminated timber beams. Eur J Wood Wood Prod 2017;75 (6):985–94.
[35] Steiger R, Gulzow A, Czaderski C, Howald MT, Neimz P. Comparison of bending stiffness of cross-laminated solid timber derived by a modal analysis of full panels and by bending tests of strip-shaped specimens. Europ J Wood Wood Product 2012;70:141–53.
[36] Li H, Wang BJ, Wang L, Wei P, Wei Y, Wang P. Characterizing engineering performance of bamboo-wood composite cross-laminated timber made from bamboo mat-curtain panel and hem-fir lumber. Compos Struct 2021;266:113785.
[37] Ozyhar T, Hering S, Niemz P. Moisture-dependent elastic and strength anisotropy of European beech wood in tension. J Mater Sci 2012;47 (16):6141–50.
[38] Ozyhar T, Hering S, Sanabria SJ, Niemz P. Determining moisture-dependent elastic characteristics of beech wood by means of ultrasonic waves. Wood Sci Technol 2012;47(2):329–41.
[39] Hopkins C. Sound Insulation. First ed:. Oxford, UK, Burlington, USA: Butterworth-Heinemann; 2007.
[40] Hopkins C, Robinson M. On the evaluation of decay curves to determine structural reverberation times for building elements. Acta Acust Acust 2013;99(2):226–44.
[41] Davy JL. Predicting the sound insulation of walls. Building Acoustics 2009;16 (1):1–20.
[42] Heckl M. Untersuchungen an Orthotropen Platten. Acust 1960;10:109–15.
[43] Ljunggren S. Airborne sound insulation of thick walls. J Acoust Soc Am 1991;89 (5):2338–45.
[44] Leppington FG, Broadbent EG, Heron KH. The Acoustic Radiation Efficiency of Rectangular Panels. Proceedings of the Royal Society London - Part A. 1982;382:245-71.
[45] Oppenheimer CH, Dubowsky S. A radiation efficiency for unbaffled plates with experimental validation. J Sound Vib 1997;199(3):473–89.

[46] Craik RJM. Sound transmission through buildings using statistical energy analysis. Aldershot: Gower; 1996.
[47] Wallace CE. Radiation Resistance of a Rectangular Panel. J Acoust Soc Am 1972;51(3B):946–52.
[48] ISO E. Acoustics — Rating of sound insulation in buildings and of building elements Part 1: Airborne sound insulation 2013.
[49] Hopkins C, Turner P. Field measurement of airborne sound insulation between rooms with non-diffuse sound fields at low frequencies. Appl Acoust 2005;66 (12):1339–82.
[50] Craik RJM, Galbrun L. Vibration transmission through a frame typical of timber-framed buildings. J Sound Vib 2005;281(3–5):763–82.
[51] Kang HJ, Ih JG, Kim JS, Kim HS. Prediction of sound transmission loss through multilayered panels by using Gaussian distribution of directional incident energy. J Acoust Soc Am 2000;107(3):1413–20.
[52] Villot M, Guigou C, Gagliardini L. Predicting the Acoustical Radiation of Finite Size Multi-Layered Structures by Applying Spatial Windowing on Infinite Structures. J Sound Vib 2001;245(3):433–55.
[53] Rhazi D, Atalla N. Transfer matrix modeling of the vibroacoustic response of multi-materials structures under mechanical excitation. J Sound Vib 2010;329 (13):2532–46.
[54] Pellicier A, Trompette N. A review of analytical methods, based on the wave approach, to compute partitions transmission loss. Appl Acoust 2007;68 (10):1192–212.
[55] Mindlin RD. Influence of rotatory Inertia and shear on flexural motions of isotropic, elastic plates. J Appl Mech 1951;1:31–8.
[56] Magrab EB. Vibrations of elastic structural members. Alphen aan den Rijn, The Netherlands: Sijthoff & Noordhoff; 1979.